

On the interpretation of the latest AMS-02 cosmic ray electron spectrum

Mattia Di Mauro,¹ Fiorenza Donato,^{2,1} and Silvia Manconi³

¹*Istituto Nazionale di Fisica Nucleare, via P. Giuria, 1, 10125 Torino, Italy*

²*Department of Physics, University of Torino, via P. Giuria, 1, 10125 Torino, Italy*

³*Institute for Theoretical Particle Physics and Cosmology,
RWTH Aachen University, Sommerfeldstr. 16, 52056 Aachen, Germany*

(Dated: October 28, 2020)

The latest AMS-02 data on cosmic ray electrons show a break in the energy spectrum around 40 GeV, with a change in the slope of about 0.1. We perform a combined fit to the newest AMS-02 positron and electron flux data using a model which includes production of pairs from pulsar wind nebulae (PWNe), electrons from supernova remnants (SNRs) and both species from spallation of hadronic cosmic rays with interstellar medium atoms. We demonstrate that the change of slope in the AMS-02 electron data is well explained by the interplay between the flux contributions from SNRs and from PWNe. In fact, the relative contribution to the data of these two populations changes by a factor of about 13 from 10 to 1000 GeV. The effect of the energy losses alone, when the inverse Compton scattering is properly computed within a fully numerical treatment of the Klein-Nishina cross section, cannot explain the break in the e^- flux data, as recently proposed in the literature.

Introduction. - The Alpha Magnetic Spectrometer (AMS-02) is a state-of-the-art particle physics detector operating on the International Space Station. By taking data since 2011, it is providing very precise measurements of cosmic-ray (CR) fluxes for leptons and nuclei, from hydrogen up to silicon, as well as for rare antiparticles such as positrons and antiprotons. Of all the CR species, electrons (e^-) and positrons (e^+) are among the most intriguing ones to study. In fact, they are probably produced by the superposition of different Galactic sources and physical production mechanisms which, due to the intense radiative losses suffered, test the properties of our Galactic environment within a few kpc.

Very recently, AMS-02 published new separate spectra for the e^+ and e^- fluxes, reaching the unprecedented energy of 830 GeV for the former and 1.2 TeV for the latter [1, 2]. The e^- data show a significant excess above about 42 GeV when compared to the trend of the spectrum at lower energies. Interestingly, the nature of this excess is different from the excess in the e^+ flux detected above 25.2 GeV which has an exponential energy cutoff at about 800 GeV. The e^- data can be well fitted by a smooth broken power law with a break at about 42 GeV and a difference of slope between the low and high-energy power laws $\Delta\gamma \approx 0.1$. By fitting the AMS-02 e^- data above 10 GeV with a single power-law and with a broken power-law function we find that the model with the break is preferred at about 5σ significance¹. Previously,

the Fermi Large Area Telescope (*Fermi*-LAT) Collaboration published the $e^+ + e^-$ inclusive spectrum from 7 GeV to 2 TeV, and reported the detection of a break at similar energies ~ 50 GeV and with $\Delta\gamma$ compatible with the one measured by AMS-02 [3]. The significance of the spectral break is at the 4σ level if the uncertainties on the energy measurements are taken into account [3].

In Ref. [4] the authors explained the *Fermi*-LAT data on the inclusive spectrum computing e^- produced by supernova remnants (SNRs) through diffusive shock acceleration, e^\pm injected in the Galaxy by pulsar wind nebulae (PWNe), and by secondary e^\pm produced in inelastic scatterings of hadronic CRs off atoms of the interstellar medium (ISM). Specifically, the hinted break in the *Fermi*-LAT e^\pm flux was well reproduced by the interplay between the SNR and the PWN components, with the latter source population emerging significantly above a few hundreds of GeV.

A recent work [5] used a similar model with PWNe, SNRs and secondary production to interpret the latest AMS-02 leptonic data. They find that the observed break in the e^- spectrum is due to an energy loss effect, specifically to the inverse Compton scattering (ICS) energy losses suffered by e^- CRs by interacting with the photons of the interstellar radiation field (ISRF). In particular, the change of slope in the data is interpreted as due by the difference between the Thompson regime and the Klein-Nishina formalism for the ICS energy losses, the former valid if $E\epsilon \ll m_e^2 c^4$, where m_e is the electron mass, E the electron energy and ϵ the photon energy in the lab

¹ We perform a fit to the data above 10 GeV using a power-law and a broken power-law functions finding a χ^2 of 39.0 and 8.7, respectively. Therefore, the $\Delta\chi^2$ between the two cases is 30.3 that, considering the two additional parameters of the broken power-law (the break and spectral index above the break), gives

a significance of 5.0 for the presence of a break in the AMS-02 e^- spectrum. We do not include in the calculation any systematic uncertainty due to energy measurement.

frame. The ISRF is composed by the Cosmic Microwave Background (CMB), and by Galactic dust emission and starlight photons which have a peak in their spectrum at about $\epsilon \approx 2.3 \times 10^{-4}/2.4 \times 10^{-3}/1.0$ eV, respectively [6]. Therefore, the observed energy break in the e^- data is found compatible with the description of the transition between the ICS losses from the Thompson regime to the Klein-Nishina formalism occurring for the starlight, at an interstellar electron energy $m_e^2 c^4/(2\epsilon) \approx 60$ GeV².

The goal of this Letter is to find an interpretation of the latest e^\pm data, and in particular to investigate if the break in the e^- AMS-02 data is explained by an energy losses effect as found in Ref. [5], or by the interplay between the emission of different source populations, similarly to what found in [4] by fitting the $e^+ + e^-$ *Fermi*-LAT data.

Models. - We employ the model already described in [4, 7, 8] (to which we refer for further details) which assumes e^\pm produced by acceleration of e^- from SNRs, pair emission from PWNe and by secondary production in the ISM. Specifically, we use the secondary production calculated in [4] by implementing the primary proton and helium spectra fitted on AMS-02 data. The spatial distributions $\rho(\mathbf{r})$ of SNRs and PWNe are modeled with a smooth function, taken from [9] for the former and [10] for the latter source population. These functions have been derived on the most updated sample of detected SNRs and pulsars (for PWNe), and corrected for source selection effects. Our source distributions are uniformly smooth in all the Galaxy, and do not account for possible single, bright sources in the few kpc around the Earth, or source stochasticity [11, 12]. We will comment on the effect of adding a spiral arm pattern in the SNR and PWN spatial distributions in the Supplemental Material; we anticipate that the main conclusions of the paper remain unchanged. We model the injection spectrum of SNRs with an energy power law with an exponential cutoff. We fix the cutoff energy at 20 TeV since there is no evidence of a cutoff in the e^- only data [2]. Instead, the PWN spectrum is calculated by taking a broken power law around $E = 500$ GeV, since the e^+ AMS-02 data shows a significant softening above a few hundreds of GeV, similarly to Ref. [5]³. Also, a broken power-law energy spectrum is suggested by multiwavelength observations of PWNe [13]. Both SNRs and PWNe are modeled as burst like events for which all e^\pm are injected in the ISM at the time of the supernova explosion.

The propagation of e^\pm in the Galactic diffusive halo,

of radius $r_{\text{disc}} = 20$ kpc and vertical half height $L \simeq 1-15$ kpc, is calculated through the transport equation:

$$\partial_t \psi - \nabla \cdot \{K(E) \nabla \psi\} + \partial_E \{b(E) \psi\} = Q(E, \mathbf{r}, t), \quad (1)$$

where $\psi = \psi(E, \mathbf{r}, t)$ is the e^\pm number density at energy E , Galactic position \mathbf{r} and time t , being the flux on Earth $\phi = v/4\pi \psi$. This differential equation accounts for the energy losses $b(E)$ due to ICS and synchrotron emission, diffusion $K(E)$ on the irregularities of the Galactic magnetic fields, and the source terms $Q(E, \mathbf{r}, t)$. Other processes usually taken into account for CR nuclei are negligible for the propagation of e^- (see, e.g., [14]). The solution of the propagation equation in Eq. 1 for a smooth distribution of sources with density $\rho(\mathbf{r})$ and Galactic SN rate Γ_* ⁴ is found, according to the semi-analytical model extensively described in [7], assuming homogeneous energy losses and diffusion:

$$\phi(\mathbf{r}_\odot, E) = \frac{v}{4\pi} \frac{\Gamma_*}{b(E)} \int dE_s Q(E_s) \times \int d^3 \mathbf{r}_s \mathcal{G}_r(\mathbf{r}_\odot, E \leftarrow \mathbf{r}_s, E_s), \rho(\mathbf{r}_s), \quad (2)$$

where $\mathcal{G}_r(\mathbf{r}_\odot, E \leftarrow \mathbf{r}_s, E_s)$ is the Green function that accounts for the probability for e^\pm injected at \mathbf{r}_s with energy E_s to reach the Earth with degraded energy E . The normalization and slope of the diffusion coefficient $K(E) = \beta K_0 E^\delta$, as well as the half-height of the diffusive halo, are taken from [15].

We assume a Galactic magnetic field of $3\mu\text{G}$ [14, 16], relevant for computing the synchrotron energy losses. As for the density of the local ISRF, we use the model published in [6]. We account for the ICS losses by numerically performing a double integral, both in the photon ϵ and electron energy E (and $\gamma = E/(m_e c^2)$), of the Klein-Nishina collision rate [17]:

$$\frac{dE}{dt} = \frac{12c\sigma_T E}{(m_e c^2)^2} \int_0^\infty d\epsilon \epsilon n(\epsilon) \mathcal{J}(\Gamma), \quad (3)$$

where $\Gamma = 4\epsilon\gamma/(m_e c^2)$, σ_T is the Thompson cross section, $n(\epsilon)$ is the ISRF spectrum and $\mathcal{J}(\Gamma)$ is defined as

$$\mathcal{J}(\Gamma) = \int_0^1 dq q \frac{2q \log q + (1+2q)(1-q) + \frac{(\Gamma q)^2(1-q)}{2(1+\Gamma q)}}{(1+\Gamma q)^3} \quad (4)$$

with $q = \epsilon/(\Gamma\gamma m_e c^2 - \epsilon)$.

We will test our model by changing the ISRF model into the ones in [5, 18], by using a spatial distribution of PWNe and SNRs containing spiral arms as in [19], and by using the diffusion parameters in [5]. In the main

² Typically, an e^- produced in the Galaxy at $E = 60$ GeV loses some 10-20% of its energy during the propagation. Therefore, an interstellar energy of 60 GeV is roughly compatible with the observed energy of the break in the AMS-02 e^- data.

³ We test also values of 300 and 700 GeV for the break and we find better fits with 500 GeV for all the tested models.

⁴ We fix $\Gamma_* = 1/\text{century}$.

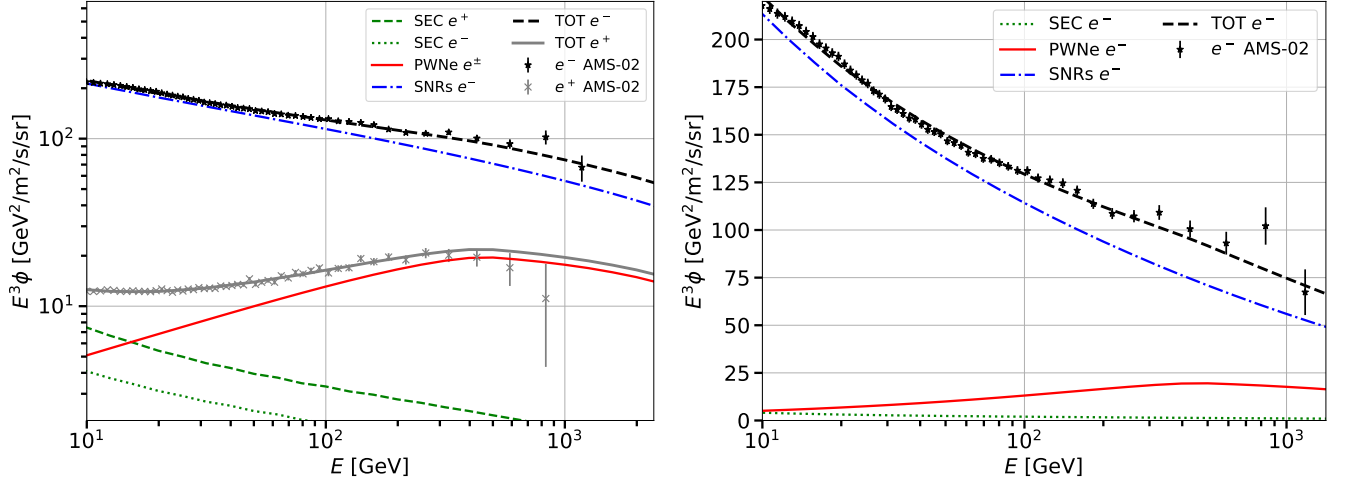


FIG. 1. Left Panel: Result for the combined fit to e^- and e^+ AMS-02 data (black and grey data points). We show the secondary production of e^+ (dashed green line) and e^- (dotted green line), e^\pm from PWNe (solid red line), e^- from SNRs (dot-dashed blue line). Right Panel: same as the left panel but zooming in the e^- sector.

part of the paper we will briefly comment our findings, while complete results are reported in the Supplemental Material.

Results. - We start by performing a combined fit to the e^+ and e^- data above 10 GeV leaving free to vary the normalization of the secondary component q , the spectral index γ_{SNR} and the SNR average energy per source W_{SNR} . The efficiency η_{PWN} for the conversion of PWN spin-down luminosity into e^\pm , and the spectral indexes γ_1 and γ_2 below and above the break for the PWN injection spectrum are left free⁵. We select data above 10 GeV to minimize the effect of the solar modulation that, if not properly taken into account, could generate a bias in the results. We thus have 6 free parameters in the fit (q , γ_{SNR} , W_{SNR} , η_{PWN} , γ_1 and γ_2), and 103 data points. The fit is performed simultaneously to e^+ and e^- data, with the scope to determine the flux of e^\pm from PWNe. We show the result of the fit in Fig. 1 along with the AMS-02 data. We find a good agreement with the high-energy part of the e^+ with $\gamma_1 = 1.88$ and $\gamma_2 = 2.31$. We need an efficiency of about $\eta_{\text{PWN}} = 0.91\%$ that is similar to the value required to explain the γ -ray halos detected in *Fermi*-LAT and HAWC data around the powerful Geminga and Monogem pulsars [21]. The best fit for the SNRs is $\gamma_{\text{SNR}} = 2.57$ and $W_{\text{SNR}} = 1.4 \cdot 10^{49}$ erg, which is compatible with our previous findings on *Fermi*-LAT e^\pm data [4], and similar to the results of Ref. [11], where we fitted AMS-02 data using also the contributions of single local SNRs. The best-fit value for q is

1.32. This implies that we have to renormalize by about 30% the predictions obtained as in [4]. The model reproduces well both the e^+ and e^- data in the entire energy range considered. Indeed, the reduced χ^2 is equal to 0.93. We argue that the break in the e^- flux data is naturally explained by the interplay of SNRs and PWNe contribution below and above the observed energy of about 40 GeV, where it has been detected by AMS-02. In order to show this more clearly, we zoom on the e^- data and the best fit model contributions in the right panel of Fig. 1. The linear scale highlights the change of slope in the data and in the model. In particular, we observe that the SNR contribution follows the data for energies between 10 to about 50 GeV. Above this energy, where the break has been detected by AMS-02, the contribution of SNRs decreases while the PWNe one increases. The SNRs, PWNe and the secondary production contribute about 96/2/2%, 92/7/1%, 78/21/1% of the total e^- flux at 10/50/400 GeV, respectively. The PWN to SNR flux relative contribution thus increases by a factor 13 from 10 GeV to 400 GeV.

Our result differs from the ones presented in Ref. [5], where the change of slope in the e^- data is ascribed to the ICS energy losses, and in particular to the change of trend due to the Klein-Nishina ICS that starts to deviate significantly from the Thompson approximation for starlight ISRF at $E > 50 - 60$ GeV. In order to test more directly their hypothesis, we have computed the energy losses for ICS off the CMB, dust emission and starlight using black body approximations of the local ISRF as in [5], which uses the black body approximation reported in [17]. We fit the ISRF in [6] with 7 black body distri-

⁵ We assume for the calculation of η_{PWN} that the average energy produced by Galactic PWNe is 10^{49} erg, as found for the pulsars in the ATNF catalog [20] with a typical pulsar decay time of $\tau_0 = 10$ kyr.

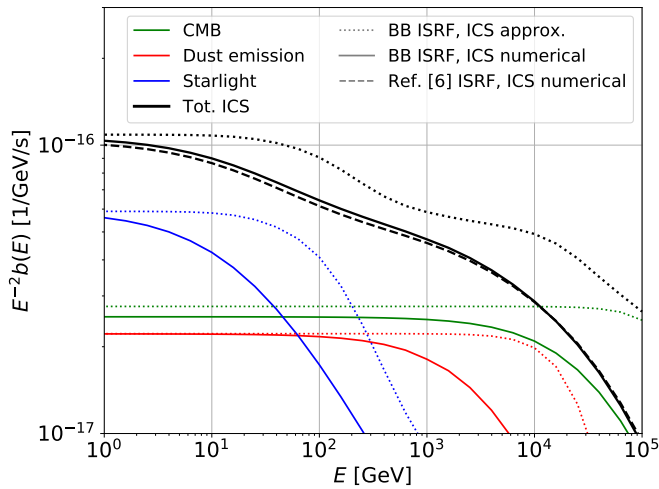


FIG. 2. Energy loss rate for ICS off the ISRF photons composed by CMB (green lines), dust emission (red lines) and starlight (blue lines), for e^\pm energy E . The total rate is shown with black lines. We report three cases: black body approximations of the ISRF and approximated Klein-Nishina calculation as in [22] (dotted lines), black body approximations of the ISRF and full numerical Klein-Nishina calculation (solid lines), ISRF as in [6] and full numerical Klein-Nishina calculation (no approximations, dashed line).

contributions (see the Supplemental Material for details)⁶. We compute the ICS losses by performing the full numerical integration of the Klein-Nishina loss rate (labeled as *ICS numerical*), or by using the approximated function as in [5], which was originally derived in [22], (labeled as *ICS approx*). We also perform the calculation using our benchmark model, i.e. by taking the exact value of the ISRF density reported in Ref. [6] at any frequency. In Fig. 2 we show the energy losses rate $b(E) = dE/dt$, multiplied by E^2 , as a function of e^\pm energy E . The energy loss rate has been obtained for each ISRF photon field, both for the approximated [22] Klein-Nishina cross section and for the full numerical integration (see Eq. 1). We also report our reference case, with the ISRF as in [6] and the full numerical Klein-Nishina implementation. It is clearly visible that the *ICS approx* cases are significantly different from the Klein-Nishina exact calculation ones for each photon field, in particular when the Thompson regime does not apply. We find that only the ICS calculated using the *ICS approx* exhibits a visible change of slope, due to the transition from the e^\pm scattering on the starlight to the one on the dust emission and CMB. On the other hand, the energy loss rates calculated performing the full numerical integration of the Klein-Nishina rate are smooth, and roughly compatible

with a power-law $b(E) \sim E^{1.9}$ from a few GeV to a few TeV. By comparing the solid and dashed black lines in Fig. 2, we also verify that using the black body approximations for the ISRF provides a loss rate very close to the one obtained with the ISRF in [6]. The difference is at most 5%.

Digging into the approximated ICS losses formulae presented in Ref. [22] and used by Ref. [5], we remind that two main simplifications were performed in order to obtain a fully analytical solution of the ICS energy losses in all the energy range.

The first relevant approximation is about the integral $\mathcal{J}(\Gamma)$, defined in Eq. 2, that in Ref. [22] is approximated as $\mathcal{J}(\Gamma) \approx 1/(9 + 2\Gamma^2)$. We verified that the ratio between $1/(9 + 2\Gamma^2)$ and the numerical integral is equal to 1 within 20% only for $\Gamma < 0.1$ and at $\Gamma \approx 3$. In the remaining range of Γ , this substitution can introduce a difference between the numerical and approximated computation of a factor of 2 for Γ around 1, and even 2-3 for $\Gamma > 10$ (see Sec. 2 of Supplemental Material). This has important repercussions on the energy loss calculation, since the function $\mathcal{J}(\Gamma)$ multiplies the total ICS energy loss rate. For example, considering the starlight component of the ISRF, peaked at about ~ 12000 K, we expect that the *ICS approx* should deviate significantly from the *ICS numerical* for $\Gamma > 0.1$, which translates to an electron energy above 5 GeV, in rough agreement to what is observed in Fig. 2 by comparing the blue solid line (*ICS numerical*) to the dotted black line (*ICS approx*). These conclusions do not depend on the ISRF modeling, as we find very similar results when using also the models reported in [5, 18]. Similar differences in the energy losses calculated with the numerical integration or approximated Klein-Nishina in [22] have been recently noted also in [23]⁷.

Finally, we verify the impact of the Klein-Nishina cross section approximated treatment in Ref. [22] with respect to the fully numerical case on the flux of e^- from SNRs. We implement the same cases reported in Fig. 2, and we fix $\gamma_{\text{SNR}} = 2.55$. The result is shown in Fig. 3. We normalize the flux of the three cases in such a way that they have the same value at 10 GeV. The *ICS approx* case provides the same flux values with respect to the other two cases - calculated with the fully numerical integration for the ISRF as a sum of black body distributions and as in Ref. [6] - at lowest and highest energies considered: 10 and 2000 GeV. Instead, it exhibits a softer spectrum between 10 and 100 GeV, and an hardening at

⁶ We checked that by using the ISRF approximation published in Ref. [17] our results are unchanged.

⁷ Just before submitting this manuscript, we got aware of the paper [24] by the same authors of Ref. [5], in which the Klein-Nishina energy losses are computed according to the more accurate approximation suggested in Ref. [23]. However, their finding that the break in the e^- flux is due to the transition of the ICS energy losses from the Thompson to the Klein-Nishina formalism is reiterated.

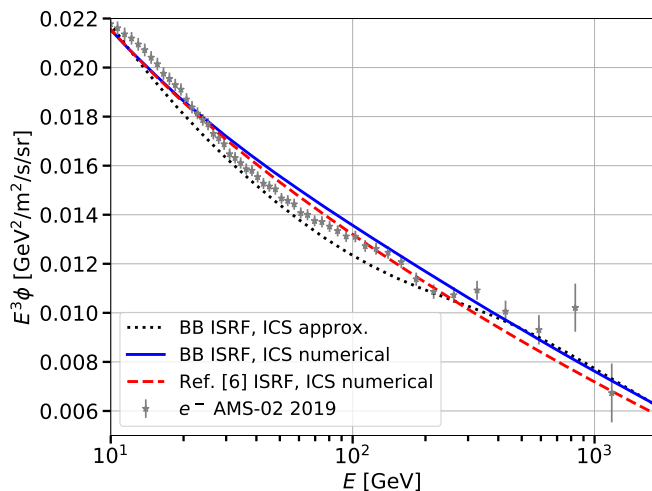


FIG. 3. Flux of e^- from a smooth distribution of SNRs calculated for $\gamma_{\text{SNR}} = 2.55$. We show the same cases for the ISRF and the Klein-Nishina energy loss rate as the ones reported in Fig. 2, in order to demonstrate the effect of the approximated calculation of the ICS energy losses published in Ref. [22] and implemented in Ref. [5] on the e^- flux.

higher energies. This spectral change makes the *ICS approx* case follow the same trend of the data between 10 and 100 GeV, and is roughly on top of the data above a few hundreds GeV. On the other hand, the flux predicted with the *ICS numerical* cases, with the black body approximation or using the [6] ISRF model, does not show any evident change of shape over the whole energy range. This finding therefore excludes the option that the break in the e^- AMS-02 data might be due to the ICS energy losses. We also test the ISRF models in [5, 18], as well as different propagation setups and spectral indexes for the SNR emission, finding similar results.

Conclusions. - In this Letter we have demonstrated that the AMS-02 e^- and e^+ flux data can be properly explained with the production of CR leptons from SNRs, PWNe and secondary production. Specifically, e^+ above 10 GeV are mostly explained with PWNe with a power-law injection spectrum broken at about 500 GeV, and a change of slope below and above the break of about $\Delta\gamma = 0.5$. SNRs explain most of the e^- flux. Their contribution decrease with energy from 96% at 10 GeV to 78% at 500 GeV, while PWNe provide an increasing contribution reaching a maximal 21% at 500 GeV. We conclude that the break measured by AMS-02 in the e^- at $E \sim 40$ GeV is very likely due to the interplay between the contribution of SNRs and PWNe. Our results differ from the one presented in Ref. [5], where the authors find that the break is due to the transition between the Thompson regime and the Klein Nishina formalism in the energy losses due to ICS. We have verified that their result are guided by the usage of the approximated form of Klein-Nishina loss rate proposed in Ref. [22], which

provides energy losses which differs by a factor of 2-3 with respect to the full numerical computation, in the relevant energy range. This cross-section approximation artificially shapes a change of slope between 20 and 1000 GeV, i.e. at energies compatible with the AMS-02 e^- spectral break.

Acknowledgements. - The work of FD has been supported by the "Departments of Excellence 2018 - 2022" Grant awarded by the Italian Ministry of Education, University and Research (MIUR) (L. 232/2016). MDM research is supported by Fellini - Fellowship for Innovation at INFN, funded by the European Union's Horizon 2020 research programme under the Marie Skłodowska-Curie Cofund Action, grant agreement no. 754496.

-
- [1] M. Aguilar, L. Ali Cavazonza, G. Ambrosi, et al. (AMS Collaboration), Phys. Rev. Lett. **122**, 041102 (2019)
 - [2] M. Aguilar, L. Ali Cavazonza, B. Alpat, et al. (AMS Collaboration), Phys. Rev. Lett. **122**, 101101 (2019)
 - [3] S. Abdollahi et al. (Fermi-LAT), Phys. Rev. D **95**, 082007 (2017), arXiv:1704.07195 [astro-ph.HE]
 - [4] M. Di Mauro et al., ApJ **845**, 107 (2017), arXiv:1703.00460
 - [5] C. Evoli, P. Blasi, E. Amato, and R. Aloisio, Phys. Rev. Lett. **125**, 051101 (2020), arXiv:2007.01302 [astro-ph.HE]
 - [6] S. Vernetto and P. Lipari, Phys. Rev. **D94**, 063009 (2016), arXiv:1608.01587 [astro-ph.HE]
 - [7] M. Di Mauro, F. Donato, N. Fornengo, et al., JCAP **1404**, 006 (2014), arXiv:1402.0321
 - [8] S. Manconi, M. Di Mauro, and F. Donato, Phys. Rev. D **102**, 023015 (2020), arXiv:2001.09985 [astro-ph.HE]
 - [9] D. Green, Mon. Not. Roy. Astron. Soc. **454**, 1517 (2015), arXiv:1508.02931 [astro-ph.HE]
 - [10] D. R. Lorimer, in *Young Neutron Stars and Their Environments*, IAU Symposium, Vol. 218, edited by F. Camilo and B. M. Gaensler (2004) p. 105, arXiv:astro-ph/0308501 [astro-ph]
 - [11] S. Manconi, M. Di Mauro, and F. Donato, JCAP **04**, 024 (2019), arXiv:1803.01009 [astro-ph.HE]
 - [12] P. Mertsch, JCAP **11**, 045 (2018), arXiv:1809.05104 [astro-ph.HE]
 - [13] A. M. Bykov, E. Amato, A. E. Petrov, A. M. Krasilchchikov, and K. P. Levenfish, Space Sci. Rev. **207**, 235 (2017), arXiv:1705.00950 [astro-ph.HE]
 - [14] C. Evoli, D. Gaggero, A. Vittino, G. Di Bernardo, M. Di Mauro, A. Ligorini, P. Ullio, and D. Grasso, JCAP **02**, 015 (2017), arXiv:1607.07886 [astro-ph.HE]
 - [15] Y. Genolini, A. Putze, P. Salati, and P. Serpico, Astron. Astrophys. **580**, A9 (2015), arXiv:1504.03134 [astro-ph.HE]
 - [16] X. Sun, W. Reich, A. Waelkens, and T. Enslin, Astron. Astrophys. **477**, 573 (2008), arXiv:0711.1572 [astro-ph]
 - [17] T. Delahaye, J. Lavalle, R. Lineros, F. Donato, and N. Fornengo, A&A **524**, A51 (2010), arXiv:1002.1910 [astro-ph.HE]
 - [18] T. A. Porter, I. V. Moskalenko, and A. W. Strong, The Astrophysical Journal **648**, L29 (2006)

ISRF	CMB	Dust emission 1	Dust emission 2	Dust emission 3	Starlight 1	Starlight 2	Starlight 3
Vernetto2016: T [K]	2.75	28	80	450	2850	6150	23210
Vernetto2016: u_γ [eV/cm ³]	0.25	0.22	0.049	0.032	0.18	0.24	0.079
Porter2006: T [K]	2.75	30	80	450	2650	5550	20210
Porter2006: u_γ [eV/cm ³]	0.25	0.36	0.049	0.032	0.30	0.20	0.051

TABLE I. This table reports the temperature and energy density u of the different black body components used to fit the ISRF model in Refs. [6] and [18], labeled as *Vernetto2016* and *Porter2006*, respectively.

-
- [19] R. J. Wainscoat, M. Cohen, K. Volk, H. J. Walker, and D. E. Schwartz, *ApJS* **83**, 111 (1992)
- [20] R. N. Manchester, G. B. Hobbs, A. Teoh, and M. Hobbs, *Astron. J.* **129**, 1993 (2005), arXiv:astro-ph/0412641
- [21] M. Di Mauro, S. Manconi, and F. Donato, *Phys. Rev. D* **100**, 123015 (2019), arXiv:1903.05647 [astro-ph.HE]
- [22] R. Schlickeiser and J. Ruppel, *New Journal of Physics* **12**, 033044 (2010), arXiv:0908.2183 [astro-ph.HE]
- [23] K. Fang, X.-J. Bi, S.-J. Lin, and Q. Yuan, (2020), arXiv:2007.15601 [astro-ph.HE]
- [24] C. Evoli, E. Amato, P. Blasi, and R. Aloisio, (2020), arXiv:2010.11955 [astro-ph.HE]
-

On the interpretation of the latest AMS-02 cosmic ray electron spectrum: Supplemental Material

BLACK BODY APPROXIMATION OF THE INTERSTELLAR RADIATION FIELD

In this Section we provide the details of the black body approximations we use to model the interstellar radiation field (ISRF). In Fig. 1 the black dashed lines illustrate the complete model for the ISRF provided by Refs. [6, 18]. The ISRF is composed by the Cosmic Microwave Background (CMB), and by Galactic dust emission and starlight photons which have a peak in their spectrum at photon energy (in the lab frame) of about $\epsilon \approx 2.3 \times 10^{-4}/2.4 \times 10^{-3}/1.0$ eV, respectively [6]. The CMB is at microwave energies instead the starlight is between the infrared, visible light and only the high energy tail above 3 eV is ultraviolet. Finally, the dust emission is produced by the star light in the optical and ultraviolet that is absorbed and re-emitted at infrared energies.

The full model for the ISRF spectrum can be fairly well approximated by a sum of black bodies spectra, each peaked at a characteristic temperature. Following the procedure performed in Ref. [17], we here introduce 7 black body distributions to model the local ISRF spectrum: one for the CMB, three for the dust emission (heated by starlight) and three for the starlight. The values of the temperature and the energy density of each component are fixed to properly fit the local Galaxy ISRF models published in [6, 18]. In Tab. I we report the values for the temperature T and the energy density u that we obtain for each of the 7 ISRF components, where $u_\gamma = \int_0^\infty \epsilon n(\epsilon) d\epsilon$ and $n(\epsilon)$ is the black body energy distribution.

In Fig. 1 we display the black body energy distributions in the approximated approach (blue dotted lines), and the results in Refs. [6, 18]. As clearly visible from this comparison, the black body method provides a very good representation of the ISRF at the peaks of the CMB, dust emission and starlight, and also at the transitions of the three components. The only part of the ISRF spectrum that the black body approximation is not able to properly capture is between $10^{13} - 10^{14}$ Hz, where the full model contains lines in the spectrum, which are associated to the absorption of star light by dust.

The difference in the inverse Compton scattering (ICS) energy loss rate by using the complete information for the ISRF density in Refs. [6, 18] or our black body approximation is at most 4-5% at low electron energy E , and basically negligible for $E > 1$ TeV. This is shown in Fig. 2 of our Letter for the ISRF model in Ref. [6], while very similar results are found also for [18].

APPROXIMATED CALCULATION OF THE INVERSE COMPTON ENERGY LOSSES

The ICS accounts for the interaction between CR e^\pm and the photons of the ISRF. Since the CMB, dust emission and starlight ISRF photons have energies at most of 1-10 eV, during these scatterings CR e^\pm lose a part of their energy, while the photon is upscattered to higher energies that are typically between the X-ray and γ -ray bands. In

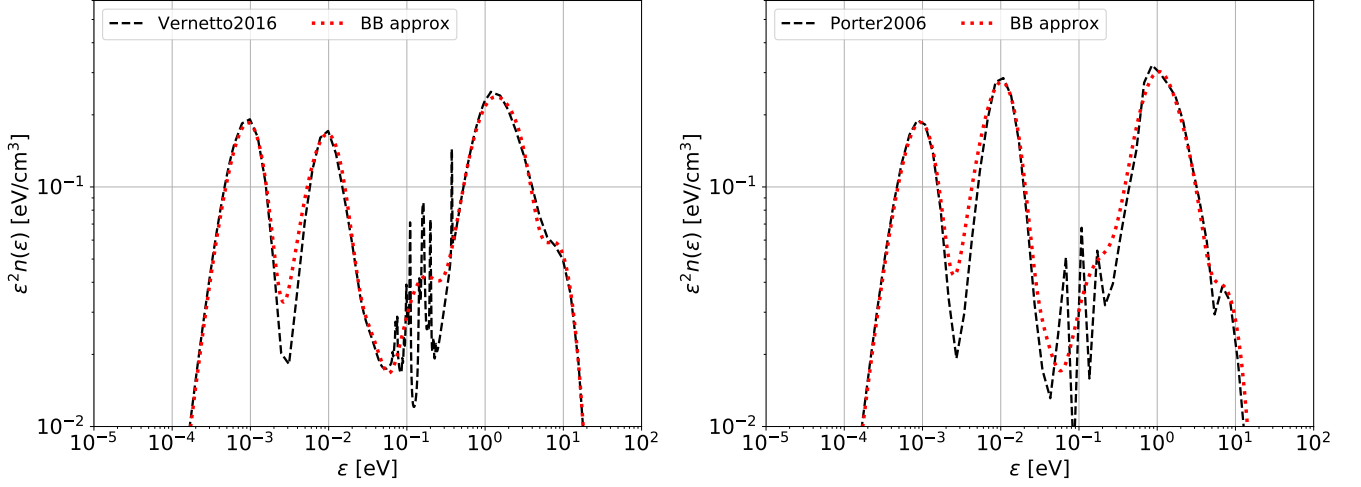


FIG. 1. Comparison between the spectrum of the ISRF density $n(\epsilon)$ published in [6] (left panel) and in [18] (right panel) with the black body approximation introduced in this paper.

the Thompson regime, that is valid for $E\epsilon \gg m_e^2 c^4$ (m_e is the electron mass), the typical energy of the scattered photons for ICS is for an head-on collision $4\gamma^2\epsilon$.

For large energies, the Thompson regime is no longer valid, and the complete calculation of the ICS energy losses requires a double integration of the Klein-Nishina cross section multiplied for the ISRF energy density $n(\epsilon)$: [17]:

$$\frac{dE}{dt} = \frac{12c\sigma_T E}{(m_e c^2)^2} \int_0^\infty d\epsilon \epsilon n(\epsilon) \mathcal{J}(\Gamma), \quad (1)$$

where σ_T is the total Thomson cross section, $\Gamma = 4\epsilon\gamma/(m_e c^2)$ and $\mathcal{J}(\Gamma)$ is defined as

$$\mathcal{J}(\Gamma) = \int_0^1 dq q \frac{2q \log q + (1+2q)(1-q) + \frac{(\Gamma q)^2(1-q)}{2(1+\Gamma q)}}{(1+\Gamma q)^3} \quad (2)$$

with $q = \epsilon/(\Gamma(\gamma m c^2 - \epsilon))$.

Ref. [22] introduced an approximated expression for Eq. 1, which allows a fully analytical solution for the energy loss rate:

$$\frac{dE}{dt} = \frac{4\sigma_T c E^2}{3(m_e c^2)^2} u_\gamma \times \mathcal{F}_{KN}(E), \quad (3)$$

where $\mathcal{F}_{KN}(E)$ is expressed as:

$$\mathcal{F}_{KN}(E) = \frac{\frac{45}{64\pi^2} (\frac{m_e c^2}{K_B T})^2}{\frac{45}{64\pi^2} (\frac{m_e c^2}{K_B T})^2 + (\frac{E}{m_e c^2})^2}. \quad (4)$$

To obtain this analytical form of the double numerical calculation of the ICS losses, Ref. [22] performed two main approximations, which we further comment in what follows.

The first and most relevant approximation concerns the integral $\mathcal{J}(\Gamma)$ (see Eq. 1 and 2) that in Ref. [22] is approximated as $J(\Gamma) \approx 1/(9 + 2\Gamma^2)$. We show in Fig. 2 the comparison between this approximation and the complete numerical calculation. The approximated function for $\mathcal{J}(\Gamma)$ works well only for $\Gamma < 0.1$ and at $\Gamma \approx 3$. In the remaining range of Γ , the parametrization with $1/(9 + 2\Gamma^2)$ can reduce the value of $\mathcal{J}(\Gamma)$ with respect to the full numerical computation by a factor of 0.5 for Γ around 1, and increases it of a factor between 2 and 7 for $\Gamma = [2, 10^3]$. In particular, considering the starlight ISRF at the peak of the energy distribution, i.e. $\epsilon \sim 1$ eV, $\Gamma > 2$ implies that the electron energy is $E > 130$ GeV. These energies for e^- are relevant for interpreting AMS-02 data.

Once the approximated value for the integral $\mathcal{J}(\Gamma)$ is introduced, a second approximation is required in order to provide the final analytical solution. Following the steps in Ref. [22], the integral over the photon energy is

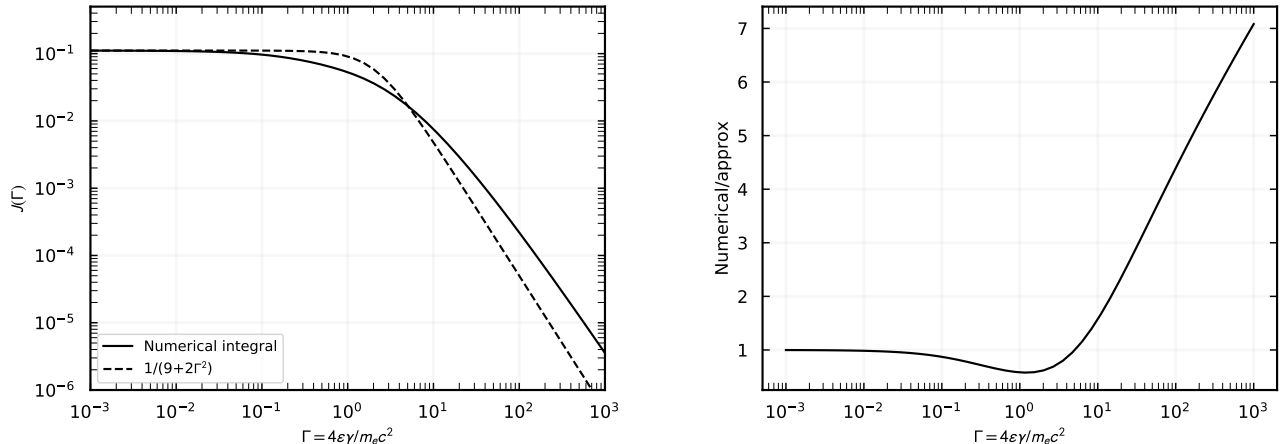


FIG. 2. The left (right) panel shows the comparison (ratio) between the numerical calculation of $\mathcal{J}(\Gamma)$ and the approximation made in [22] as a function of Γ .

parametrized as a function of the variable $A = \frac{3m_e c^2}{\sqrt{32} K_B T \gamma}$. If the leading contributions for both regimes of small and large A are considered, an approximation of at most a factor of two for $A \sim 1$ is further introduced.

As already commented in the main text, these differences can have significant repercussions on the energy loss rate calculation.

RESULTS OF THE ANALYSIS WITH DIFFERENT MODEL ASSUMPTIONS

In the main paper, the model for the production and propagation of e^\pm to the Earth is based on the following choices: the ISRF is taken from [6], the spatial distribution of SNRs and PWNe is smooth without spiral arms structures, and the diffusion coefficient parameterization is taken from [15]. In this section we show the results obtained with a combined fit to the combined e^+ and e^- data when changing these assumptions. We test our model by using the ISRF models published in [5, 18]. We will label these two cases into *Porter2006* and *Evoli2020*. We also add the spiral arms structures for the PWN and SNR spatial distributions using the model in [19], as already implemented and discussed in Ref. [4]. This case is named as *Spiral Arms*. Finally, we assume the Galactic diffusion parameters used in [5], where the diffusion coefficient is modeled as a broken power law (*BPLDiffusion*). In Tab. II we summarize the results of our additional fits on different scenarios regarding the ISRF and propagation models, the presence or not of spiral arms shaping the distribution of sources, and the fully numerical or approximated analytical formulae for the Klein-Nishina cross section. We report the best-fit values for the renormalization factor of the secondary source term, the SNR spectral indexes γ_{SNR} , the average energy emitted per source W_{SNR} , the PWN spectral indexes γ_1 and γ_2 below and above the break energy, the PWN conversion efficiency η_{PWN} and the combined e^- and e^+ reduced chi-squared $\tilde{\chi}^2$ for the best fit.

We find that all the tested cases with spiral arms produce harder SNR and PWN spectral indexes. When we perform the numerical integration of the Klein-Nishina ICS energy loss rate we find renormalization of the secondary production of about 30%, while with the approximated formula in [22], and used in [5] we need an higher factor of almost 80%. Changing the ISRF model between [5, 6, 18] provides similar values for the parameters and goodness of fit. The ISRF of Ref. [6] gives slightly better fits with respect to the other two ones. Assuming the *BPLDiffusion* propagation model [5] we find slightly better fits, and with very similar best-fit parameters, with respect to using the propagation parameters in [15]. Depending on the spectral index of the SNR population, also the *BPLDiffusion* introduces a mild change of slope in the propagated spectrum at high energies. The case that produces the lowest $\tilde{\chi}^2$ is with the ISRF and propagation parameters as in [5], and with the approximated ICS energy losses of [22]. However, we remind that this case is driven by an approximated version of the ICS losses that poorly reproduces the transition between the Thompson regime and the Klein-Nishina formalism. Moreover, the $\tilde{\chi}^2$ values obtained for the different cases are very similar, and none is significantly better than the others from a statistical point of view. Finally, we remind here that this $\tilde{\chi}^2$ is obtained with a combined fit to e^+ and e^- data and that the focus of this paper has been

ISRF	Propagation	Spiral Arms	ICS	q	γ_{SNR}	W_{SNR} [10^{49} erg]	$\gamma_{1,2}$	η_{PWN}	$\tilde{\chi}^2$
Vernetto2016	Genolini2015	No	numerical	1.32	2.57	1.35	1.88/2.31	0.009	0.93
Vernetto2016	Genolini2015	Yes	numerical	1.54	2.42	1.51	1.61/2.20	0.017	1.64
Porter2006	Genolini2015	No	numerical	1.35	2.58	1.23	1.88/2.23	0.008	1.00
Evoli2020	Genolini2015	No	numerical	1.31	2.59	1.42	1.90/2.27	0.009	0.97
Vernetto2016	BPLDiffusion	No	numerical	1.33	2.50	1.14	1.80/2.58	0.010	0.82
Evoli2020	BPLDiffusion	Yes	approx	1.78	2.43	2.11	1.56/2.80	0.018	0.71

TABLE II. Summary of the results obtained with the combined fit to e^\pm AMS-02 data as described in the main part of the letter. We show cases where we vary the ISRF model, diffusion parameters, where we include or not the Spiral arms, and use the numerical calculation of the Klein-Nishina ICS energy losses or employ the approximated version presented in [22]. We list the best-fit values for the secondary renormalization q , SNR spectral index γ_{SNR} and average energy emitted per source W_{SNR} , PWN spectral indexes γ_1 and γ_2 below and above the break energy, the PWN efficiency η_{PWN} and the value of the obtained reduced chi-square ($\tilde{\chi}^2$).

on the e^- flux.

In Fig. 3 we show the result on e^- flux at Earth for the six cases tested in this Section and summarized in Tab. II. If we only modify the ISRF model or propagation parameters, we obtain very similar contributions from the SNR and PWN fluxes. Instead, if we use the ICS energy losses approximation as in [22] then also used in [5], we find a change of trend in the SNR flux at around 100 GeV, similary to what found in [5]. In particular, since the SNR flux for this model shows an hardening with increasing energy, the PWN contribution is forced to be slightly lower than in the other cases, and the resulting fit is better. However, as demonstrated in the Letter, this model is based on an approximated calculation of the Klein-Nishina ICS energy losses, which we have shown to be reliable only for some regimes of the electron and background photon energies. The benchmark model we have presented in the Letter, in which energy losses are computed using a fully numerical approach, fits very well the data.

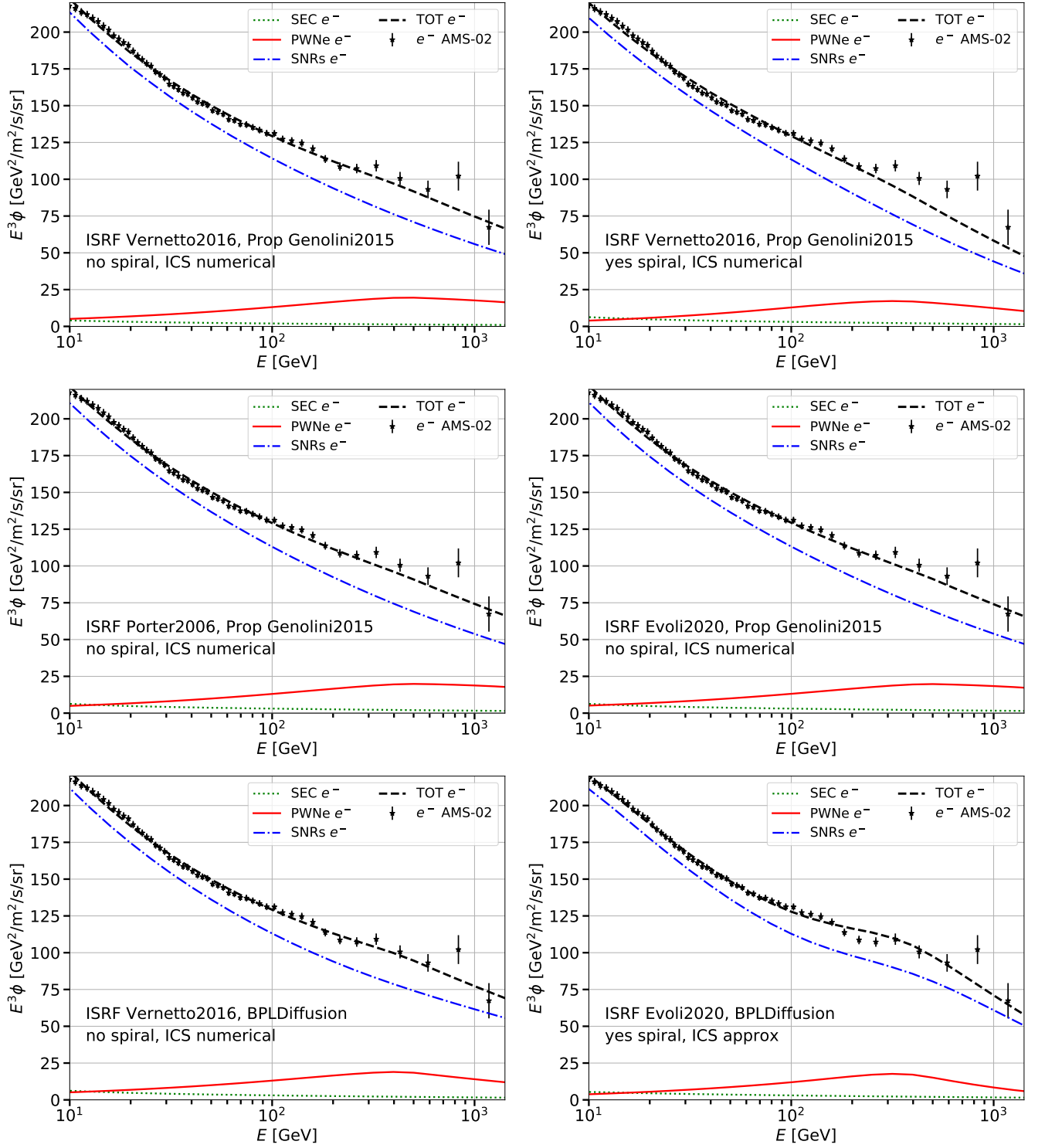


FIG. 3. Flux of e^- from SNRs (blue dot-dashed line), PWNe (red solid line) and secondary production (green dotted line) as derived from a combined fit to the e^\pm AMS-02 data. We also show the total contribution (black dashed line) and the AMS-02 data (black data points). Each plot represents one case reported in Tab. II.